13th ewtec 2019 Proceedings of the 13th European Wave and Tidal Energy Conference 1-6 Sept 2019, Naples, Italy

Evaluation of the forecasting model for wave climate prediction at DanWEC

Amélie Têtu and Jens Peter Kofoed

Abstract—. **In the process of setting up the Danish test site for wave energy Aalborg University and DHI have collaborated with DanWEC to provide dedicated descriptions of the wave climate at the site by hindcast wave modelling and setting up a forecast system. A hindcast model was developed in an effort to obtained a detailed assessment of the wave climate at the test site. The hindcast model is based on DHI's MIKE 21 spectral wave model and this model was also applied as the basis for setting up a forecast service. The forecast updates a range of parameters related to the wave conditions, wind conditions and current speed throughout the modelling area twice every 24 hours and provides a 5½ days prognostic of the conditions at the test site. This work will give an introduction to the test site and the hindcast model which is used as base for the forecast model. The forecast system and the ability of the forecast to predict accurately the wave conditions at the test site will then be presented. A detailed analysis of its accuracy in terms of different error metrics with respect to measurements of wave height from wave measuring buoys deployed at the test site has been performed and is also included in this work.**

Keywords—**Wave energy, forecast model, levelised cost of energy, O&M**

I. Introduction

IN response to the political energy policies on the global level, a race has been initiated for renewable energy sources to become primary, and in some case the only, source of energy in some decades. To attain this goal, a drastic increase of renewable energy deployment and a diversification of the energy mix are compulsatory. Wave energy is considered as a candidate to enter the energy mix as it has complementary advantages with respect to both wind energy and photovoltaics. In order to bring wave energy to the level needed for deployment, lower levelised cost of energy (LCoE) is required. Similarly to wind energy, reduction of operation and maintenance (O&M) associated costs is believed to have a major effect on the LCoE. One strategy to reduce the O&M cost is to improve forecast models in order to better predict weather windows in terms of duration and wave height levels. This strategy has been implemented at a smaller scale at the Danish wave energy center (DanWEC) [1] located at the northwestern coast of mainland Denmark. In collaboration with the department of civil engineering at Aalborg University and DHI, a forecast model for the test site area was developed based on the MIKE 21 spectral wave model [2],[3]. The forecast model predicting the weather windows was established as a support tool for both the staff at the test site and the wave energy converter developers testing in the area [4].

In this work the forecast model developed for DanWEC will be presented. It updates a range of parameters related to the wave conditions, wind conditions and current speed throughout the modelling area twice every 24 hours. The forecast model provides a 5½ days prognostic of the conditions at the test site and the model forcing comprises input from regional DHI models and wind fields.

First an introduction to the test site and its sensor network will be given. The hindcast model which is used as base for the forecast model will be introduced together with validation of the model against data from wave measuring buoys. The forecast system and the ability of the forecast to predict accurately the wave conditions will then be presented. Its accuracy in terms of prediction errors with respect to measurements of wave height from wave measuring buoys deployed at the test site will also be given. The detailed analysis of the accuracy of the forecast model will be given for a period of two years, where seasonal variations were also investigated.

II. Danish wave energy center

A. Description of the test site

The DanWEC test site is situated on the North-West coast of the Danish peninsula Jutland, at Hanstholm, facing the Danish part of the North Sea. The data acquisition network of the test site comprises three buoys, as shown in Fig. 1. It consists of one Datawell Mark II non

Paper ID: 1512, Conference track: ONM

Amélie Têtu is with the Ocean and coastal engineering research group at the Department of Civil Engineering, Aalborg University, Thomas Manns Vej 23, 9220 Aalborg, Denmark. (e-mail: at@civil.aau.dk)

Jens Peter Kofoed is with the Ocean and coastal engineering research group at the Department of Civil Engineering, Aalborg University, Thomas Manns Vej 23, 9220 Aalborg, Denmark. (e-mail: jpk@civil.aau.dk)

Fig. 1. DanWEC network sensor situated on the north-west coast of mainland Denmark.

directional buoy, placed outside Hantsholm's harbour, and two Datawell DWR4 directional buoys including current measurements. The non-directional buoy Buoy I has been installed in 1998 and has provided almost 20 years of data [5]. Before 1998 a similar older version of a wave rider buoy was placed outside the harbour and paper records of wave data over the period 1979-1988 was analysed in relation to the first Wave Power experiments by Danish Wave Power Aps in 1989 [5].

The two DanWEC directional buoys were installed in March 2015 and have been providing new information on the wave climate at this location, including insight on the directionality of the waves, the wave spectra and current characteristics. The two directional buoys are situated at a distance of approximately 3 km from the shore and are equipped with accelerometers providing displacements over time after proper filtering and double integration. The accelerometer measuring the vertical displacement is placed on a gravity-stabilized platform, decoupling the movement of the buoy from the measurement of the wave height through vertical acceleration. The directional buoys are also equipped with three acoustic current transducers placed 120° laterally apart. They measure the Doppler shift of reflected 2 MHz pings at roughly 1 m water depth. All directions are measured relative to the north magnetic pole as both systems are equipped with a magnetic compass. The directional buoys measure the north, west and vertical displacements at a rate of 2.56 Hz and the raw data is transferred to a computer onshore through a radio link signal. The current measurement is taken every 10 minutes and is sent by radio link signal to the same computer onshore. The raw data is processed with Datawell Waves4 software suite [6]. Fourier analysis is used to obtain the spectral parameters from the horizontal and vertical displacements over a period of 30 minutes. Frequency-domain parameters are available for Buoy I, II, and III [3].

The water depth in the test site varies from 15 meter closest to the coast to about 25 meter at the deepest. In general the seabed is covered with sand and silt, however at some locations this cover is washed away and the chalk is exposed. DanWEC has carried out a geotechnical survey of the test area which defines the water depth variation as well as the typical variation of the sediments. This information is made available for developers that enter a testing agreement with DanWEC.

Wind data is also available for the location. It is measured using an anemometer located at the Port of Hanstholm. The data is continuously transmitted to www.hyde.dk and is added to the DanWEC database.

III. Wave Climate Model for DanWEC

The forecast model for the DanWEC test site has been based on the hindcast model for the area. The later will be introduced together with its validation against data from wave measuring buoys. The forecast model will afterwards be presented.

B. Hindcast model

The forecast model is based on a hindcast model of the DanWEC test site. For the hindcast model the numerical model used is the MIKE 21 Spectral Wave (SW) model version 2016 [7]. MIKE 21 SW includes the following physical phenomena:

- Wave growth by action of wind
- Non-linear wave-wave interaction (quadruplet and triad-wave interactions)
- Dissipation due to white-capping
- Dissipation due to bottom-friction
- Dissipation due to depth-induced wave breaking
- Refraction and shoaling (due to depth variations and currents)
- Wave-current interaction
- Effect of time-varying water depth and currents

Wave diffraction and wave reflection are not included in this study as no island, headland or other obstruction are present in the area under study. The effect of ice coverage on the wave field is also not relevant for the area under study. The frequency discretization was 25 bins

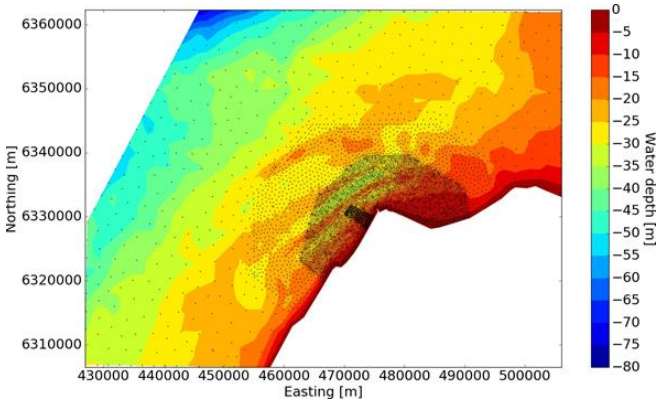

Fig. 2. Bathymetry and mesh resolution used in MIKE 21 Spectral Wave model to obtain the 35 years hindcast data at the DanWEC test site.

with a minimum frequency of 0.033 Hz and a logarithmic frequency increment factor of 1.15 resulting in resolved wave periods in the interval [1.2, 33.3] s ([0.033, 0.945] Hz).

The output wave data covers the period from January 15, 1981 to December 31, 2015, a total of 35 years. The number of azimuthal directions in the numerical model is 24. A maximum (adaptive) computational time step of 300 s was applied and the output time step is 1 hour. The bathymetry and grid resolution used in the numerical model are presented in Fig. 2.

Wind forcing was applied with an uncoupled air-sea interaction process. The wind energy momentum transfer to the water was calibrated through the Charnock parameter, which directly influences the amount of energy transferred from the wind to the build-up waves. A Charnock parameter of 0.0185 was applied, which is commonly used for coastal areas. A cap was introduced for the ratio of friction velocity to wind speed ($U/U10$) [8]. The cap was set at 0.055 [8]. This cap limits the momentum transfer and is based on the documented concept of a saturation of the drag coefficient at extreme storm wind speeds.

Depth-induced wave breaking is a process by which waves dissipate energy when the waves are too high to be stable at the local water depth, i.e. exceeding a limiting wave height to depth ratio. The breaking parameter, γ, varies significantly depending on the wave conditions and the bathymetry. The γ parameter controlling the limiting water depth and the α parameter controlling the rate of dissipation were applied with the default (average) values of $\gamma = 0.8$ and $\alpha = 1$ (see [9, 10]).

Bottom friction was described through the Nikuradse roughness, meaning that the bottom friction varies with the orbital characteristics of the wave close to the bottom. The applied roughness was $k_N = 0.04$ m.

For the boundary conditions, spectral wave data from the Spectral Wave model Northern Europe (SWNE) is applied along the open boundaries. The SWNE was validated with data from two different stations: Fjaltring NE and Hirtshals west. This model takes into account coastal reflections. More information is available in [11].

White-capping, a process by which waves dissipate energy, is primarily controlled by the steepness of the waves. The C_{dis} coefficient is a proportional factor on the white-capping dissipation source function and thus controls the overall dissipation rate. The $DELTA_{dis}$ coefficient controls the weight of dissipation in the energy/action. These parameters were found from calibration, and are within the range of typically adopted parameters in coastal applications.

The hindcast model was validated against wave measurements from Buoy I, Buoy II and Buoy III and the results from the validation can be found in [11]. As an example, a very good agreement between measured and modelled data is shown in Fig. 3 where a snap shot in time between the 12th of September 2015 and the 9th of October 2015 is taken.

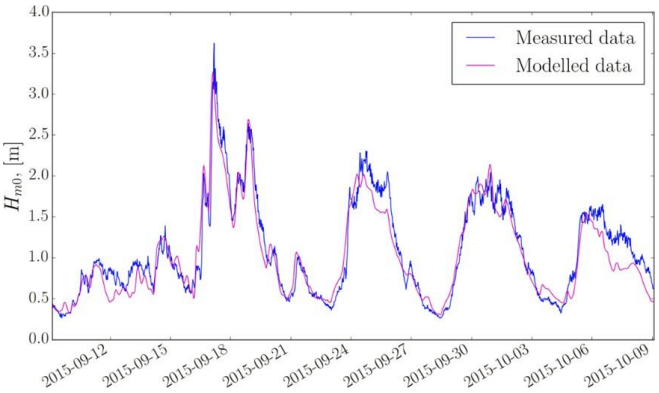

Fig. 3. Measured and modelled data between the 12th of September 2015 and the 9th of October 2015 at the reference point.

C. *Forecast model*

The forecast model for the DanWEC test site is based on the hindcast model where the grid output resolution is reduced as shown in Fig. 4. The forecast model updates a 5½ days-horizon twice every 24 hours [4]. The model forcing comprises input from regional DHI models and forecast wind fields. Some of the parameters given by the forecast model are listed in Table I.

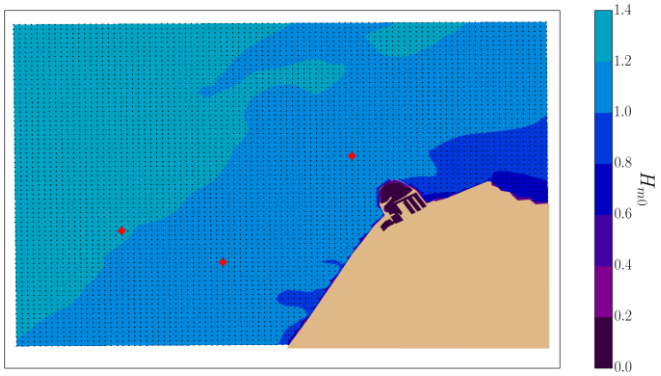

Fig. 4. Example of forecast H_{m0} for the total area provided for the forecast model at DanWEC. The three markers mark the position of the wave measuring buoys and the dots correspond to the mesh of the model, i.e. values for each point can be extracted.

TABLE I
LIST OF OUTPUT PARAMETERS FOR THE FORECAST MODEL UPDATED TWICE EVERY 24 HOURS THROUGHOUT THE MODELLING AREA (FIG.4)

Symbol	Quantity	Unit
H_{m0}	Significant wave height	[m]
H_{max}	Maximum wave height	[m]
T_p	Peak wave period	[s]
T_{01}	Spectral mean period	[s]
T_{02}	Mean zero-upcrossing period	[s]
θ	Mean wave direction	[°]
U	Wind speed	[m·s^{-1}]
v	Current speed	[m·s^{-1}]

D. *Forecast model validation*

In other to validate the forecast model, each forecast time series between the period January 2017 and December 2018 has been compared with observed data for the corresponding period. Fig. 5 shows an example of a H_{m0} time series comparison

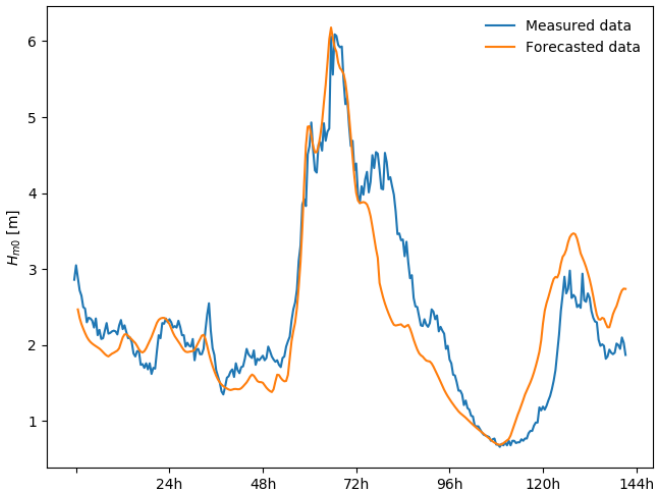

Fig. 5. Example of time series for measured values and forecast of H_{m0} over the whole forecast horizon.

between observed data and forecasted data. Note that the first 12 hours correspond to hindcast data.

In Fig. 6, the forecast horizon is divided into 4 timeframes, where the first 12 hours have been removed, and the forecasted data for H_{m0} is presented as a function of the observed data. Horizon 1 corresponds to the timeframe [0, 36] hours, Horizon 2 to]36, 72] hours, Horizon 3 to]72, 108] hours and Horizon 4 to]108, 144] hours. A 1:1 dotted-line is also shown in the figure to better qualify the agreement between the observed and forecasted data. The respective figure for T_p is presented in Fig. 7.

As expected for both H_{m0} and T_p, the prediction is better for the Horizon 1, corresponding to the first 36 hours. The second thing easy to notice is that the prediction for H_{m0} is more accurate than for T_p. It can also be noticed from Fig. 6 that there is a negative bias for large event, i.e. the model is somehow underpredicting high H_{m0} events. This effect is easier to appreciate further in the forecast horizon, especially Horizon 3 and 4.

For the accuracy analysis, the following error metrics have been used, defined in terms of the forecast data ($\hat{x}$), the observed data (x) and the number of validation points (N_v):

$\bar{\hat{x}}$ stands for the average of the forecast data $\hat{x}$:

$$\bar{\hat{x}} = \frac{1}{N_v}\sum_{i=1}^{N_v}\hat{x}_i$$

while $\bar{x}$ is the average of the observed data:

$$\bar{x} = \frac{1}{N_v}\sum_{i=1}^{N_v}x_i$$

AME is the absolute mean difference defined as:

$$AME = \frac{1}{N_v}\sum_{i=1}^{N_v}|\hat{x}_i - x_i|$$

MBE is the mean bias error:

$$MBE = \frac{1}{N_v}\sum_{i=1}^{N_v}(\hat{x}_i - x_i)$$

$RMSE$ is the root mean squared error:

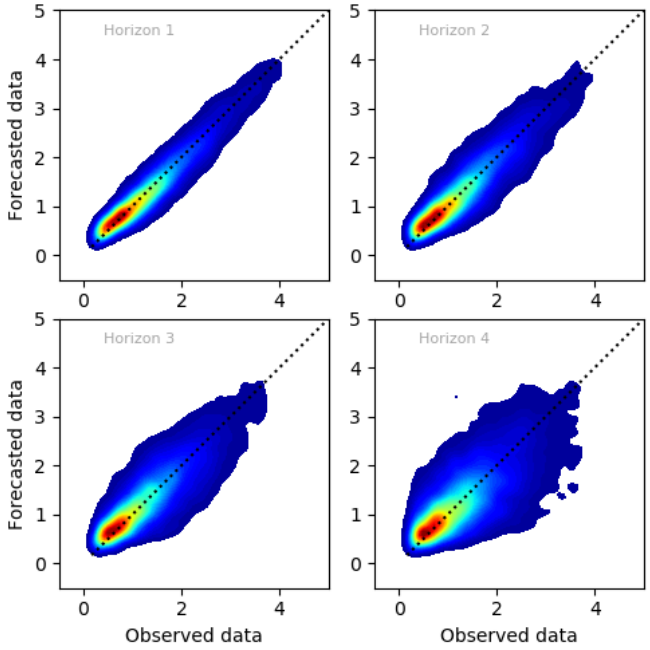

Fig. 6. Forecasted data as a function of observed data for H_{m0} for the total period corresponding to pair of points. The forecast horizon is divided into 4: Horizon 1 corresponds to timeframe [0, 36] hours, Horizon 2 to]36, 72] hours, Horizon 3 to]72, 108] hours and Horizon 4 to]108, 144] hours. The dotted line corresponds to a 1:1 line.

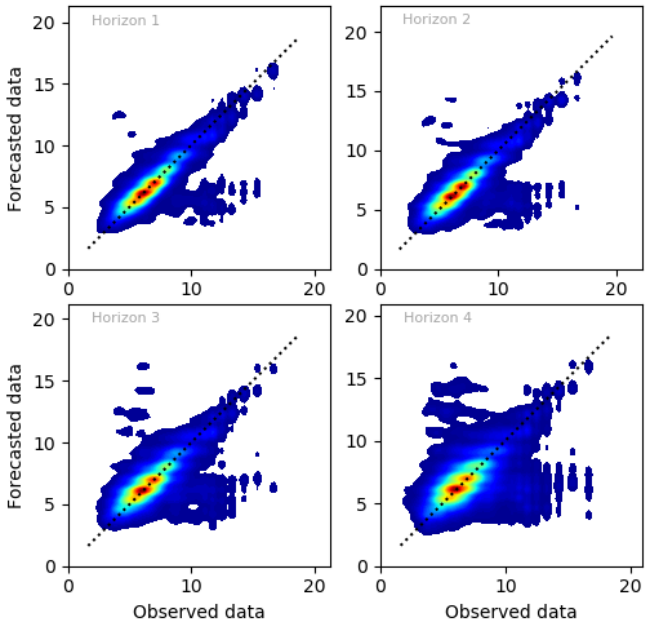

Fig. 7. Forecasted data as a function of observed data for T_p for the total period corresponding to pair of points. The forecast horizon is divided into 4: Horizon 1 corresponds to timeframe [0, 36] hours, Horizon 2 to]36, 72] hours, Horizon 3 to]72, 108] hours and Horizon 4 to]108, 144] hours. The dotted line corresponds to a 1:1 line.

$$RMSE = \sqrt{\frac{1}{N_v}\sum_{i=1}^{N_v}(\hat{x}_i - x_i)^2}$$

R^2 is the coefficient of determination:

$$R^2 = 1 - \frac{\sum_{i=1}^{N_v}(x_i - \hat{x}_i)^2}{\sum_{i=1}^{N_v}(x_i - \bar{x})^2}$$

SI is the scatter index:

$$SI = \frac{RMSE}{\bar{x}}$$

$MARE$ is mean absolute percentage error:

$$MARE = \frac{100}{N_v}\sum_{i=1}^{N_v}\left|\frac{x_i - \hat{x}_i}{x_i}\right|$$

$RRMSE$ is the relative root mean squared error:

$$RRMSE = \frac{100}{\bar{x}}\sqrt{\frac{1}{N_v}\sum_{i=1}^{N_v}(x_i - \hat{x}_i)^2}$$

$RMSRE$ is the root mean squared relative error:

$$RMSRE = \sqrt{\frac{1}{N_v}\sum_{i=1}^{N_v}\left(\frac{x_i - \hat{x}_i}{x_i}\right)^2}$$

All those error metrics were compiled as a function of the time horizon of the forecast. While AME, MBE and $RMSE$ have the same units as the observed/forecast parameter, R^2, SI, $MARE$, $RRMSE$ and $RMSRE$ are all relative error metrics and can thus be used to compare performance between different parameters.

Table II and III show the errors metrics for H_{m0} and T_p, respectively. One thing to notice from the tables is that the forecast model as a negative mean bias error, meaning that the model is predicting lower values of both H_{m0} and T_p throughout the forecast horizon, as it could also be seen in Fig. 6 and 7. The error metrics are also showing that the forecast model has higher accuracy the closer it is to the actual time. The model is also predicting more accurately wave heights than wave periods.

E. *Seasonal variations*

The time series were divided into seasons to grasp seasonal variations for the forecast model. The seasons are defined as: winter includes the months of December, January and February; spring includes the months of March, April and May; summer includes the months of June, July and August; and includes the months of September, October and November. Fig. 8 shows the equivalent of Fig. 6 for the winter season and Tables IV, V, VI, and VII show the error metrics for the winter, spring, summer and autumn seasons, respectively, for H_{m0}.

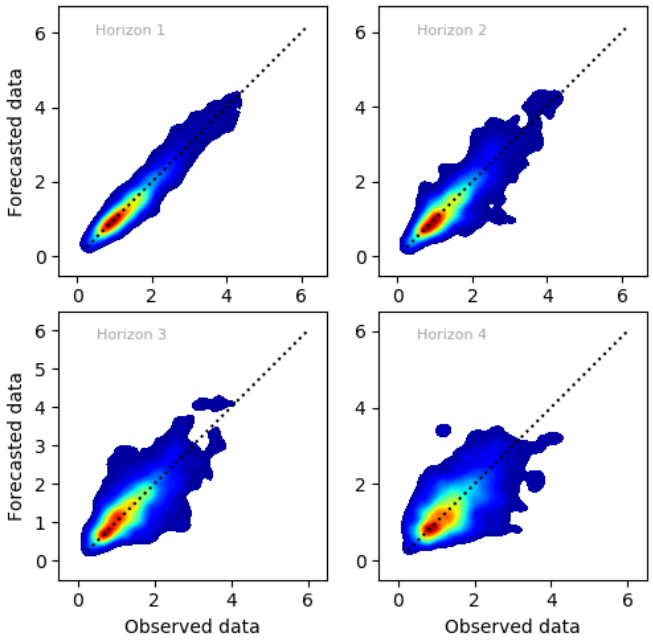

Fig. 8. Forecasted data as a function of observed data for H_{m0} for the winter months. The forecast horizon is divided into 4: Horizon 1 corresponds to timeframe [0, 36] hours, Horizon 2 to]36, 72] hours, Horizon 3 to]72, 108] hours and Horizon 4 to]108, 144] hours. The dotted line corresponds to a 1:1 line.

TABLE II
ERRORS METRICS FOR H_{m0} FOR THE WHOLE PERIOD, WHERE $N_v = 424$.

H_{m0} ($N_v = 424$)								
	AME [m]	MBE [m]	$RMSE$ [m]	R^2 [-]	SI [-]	$MARE$ [%]	$RRMSE$ [%]	$RMSRE$ [-]
18h	0.169	-0.045	0.239	0.929	0.151	11.72	15.08	0.154
36h	0.209	-0.042	0.287	0.902	0.181	14.50	18.11	0.199
54h	0.281	-0.058	0.428	0.778	0.271	18.67	27.06	0.262
72h	0.323	-0.070	0.503	0.704	0.318	21.10	31.75	0.289
90h	0.351	-0.042	0.514	0.673	0.327	23.58	32.69	0.335
108h	0.367	-0.052	0.528	0.653	0.336	25.95	33.61	0.360
126h	0.444	-0.031	0.639	0.487	0.409	32.82	40.91	0.489
144h	0.509	-0.056	0.690	0.353	0.446	38.19	44.56	0.588

TABLE III
ERRORS METRICS FOR T_p FOR THE WHOLE PERIOD, WHERE $N_v = 424$.

T_p ($N_v = 424$)								
	AME [s]	MBE [s]	$RMSE$ [s]	R^2 [-]	SI [-]	$MARE$ [%]	$RRMSE$ [%]	$RMSRE$ [-]
18h	1.132	-0.192	2.096	0.327	0.266	14.11	26.62	0.267
36h	1.215	-0.083	2.323	0.230	0.297	16.60	29.66	0.353
54h	1.390	-0.269	2.419	0.158	0.306	17.45	30.64	0.307
72h	1.306	-0.210	2.297	0.257	0.293	16.85	29.27	0.295
90h	1.651	-0.085	2.755	-0.176	0.352	21.67	35.19	0.382
108h	1.751	-0.099	2.932	-0.199	0.372	22.79	37.23	0.398
126h	1.844	-0.190	2.902	-0.257	0.371	23.86	37.10	0.386
144h	1.919	-0.242	2.959	-0.218	0.376	24.51	37.65	0.390

TABLE IV
ERRORS METRICS FOR H_{m0} FOR THE WINTER MONTHS, WHERE $N_v = 228$.

H_{m0} ($N_v = 228$)								
	AME [m]	MBE [m]	$RMSE$ [m]	R^2 [-]	SI [-]	$MARE$ [%]	$RRMSE$ [%]	$RMSRE$ [-]
18h	0.167	-0.034	0.246	0.936	0.150	10.65	15.03	0.137
36h	0.206	-0.028	0.283	0.919	0.173	13.98	17.33	0.199
54h	0.318	-0.077	0.493	0.748	0.299	19.89	29.89	0.279
72h	0.371	-0.088	0.606	0.637	0.365	22.28	36.48	0.313
90h	0.399	-0.074	0.591	0.616	0.360	24.73	36.00	0.346
108h	0.390	-0.069	0.582	0.616	0.361	26.91	36.13	0.374
126h	0.463	-0.043	0.671	0.485	0.418	33.82	41.82	0.514
144h	0.502	-0.070	0.666	0.414	0.416	36.70	41.63	0.522

TABLE V
ERRORS METRICS FOR H_{m0} FOR THE SPRING MONTHS, WHERE $N_v = 322$.

H_{m0} ($N_v = 322$)								
	AME [m]	MBE [m]	$RMSE$ [m]	R^2 [-]	SI [-]	$MARE$ [%]	$RRMSE$ [%]	$RMSRE$ [-]
18h	0.168	0.002	0.219	0.925	0.185	19.28	18.48	0.283
36h	0.186	0.011	0.249	0.888	0.214	20.17	21.44	0.276
54h	0.225	0.038	0.320	0.835	0.278	24.99	27.80	0.357
72h	0.263	0.026	0.358	0.753	0.318	28.02	31.84	0.393
90h	0.293	0.043	0.413	0.714	0.366	33.00	36.64	0.489
108h	0.307	0.028	0.437	0.652	0.385	32.08	38.51	0.457
126h	0.379	0.049	0.548	0.502	0.483	41.68	48.28	0.684
144h	0.414	0.050	0.600	0.314	0.539	46.04	53.92	0.764

TABLE VI
ERRORS METRICS FOR H_{m0} FOR THE SUMMER MONTHS, WHERE $N_v = 236$.

H_{m0} ($N_v = 263$)								
	AME [m]	MBE [m]	$RMSE$ [m]	R^2 [-]	SI [-]	$MARE$ [%]	$RRMSE$ [%]	$RMSRE$ [-]
18h	0.140	-0.029	0.187	0.939	0.146	13.56	14.63	0.188
36h	0.195	-0.045	0.264	0.874	0.205	17.43	20.54	0.237
54h	0.211	0.010	0.287	0.854	0.222	20.35	22.16	0.307
72h	0.247	0.016	0.338	0.793	0.264	23.81	26.36	0.369
90h	0.300	0.027	0.426	0.697	0.329	28.56	32.90	0.432
108h	0.339	-0.003	0.478	0.616	0.367	32.17	36.70	0.515
126h	0.399	-0.041	0.566	0.476	0.434	37.64	43.45	0.615
144h	0.486	-0.042	0.676	0.239	0.525	48.51	52.51	0.806

TABLE VII
ERRORS METRICS FOR H_{m0} FOR THE AUTUMN MONTHS, WHERE $N_v = 330$.

H_{m0} ($N_v = 330$)								
	AME [m]	MBE [m]	$RMSE$ [m]	R^2 [-]	SI [-]	$MARE$ [%]	$RRMSE$ [%]	$RMSRE$ [-]
18h	0.167	-0.066	0.230	0.946	0.140	11.78	13.97	0.155
36h	0.200	-0.073	0.279	0.917	0.170	13.40	16.95	0.176
54h	0.241	-0.037	0.364	0.858	0.223	15.66	22.26	0.218
72h	0.264	-0.043	0.379	0.847	0.230	17.47	23.00	0.238
90h	0.298	-0.021	0.440	0.799	0.265	18.81	26.46	0.267
108h	0.367	-0.050	0.517	0.720	0.309	23.07	30.86	0.313
126h	0.420	-0.089	0.619	0.602	0.369	26.70	36.86	0.389
144h	0.496	-0.111	0.712	0.477	0.419	30.44	41.90	0.422

Tables IV shows the same tendencies as seen previously for the whole period (Table II). A negative mean bias error is observed for the winter months and the error on the forecasted with respect to the observed data is increasing as getting further into the horizon. For the spring months, the values of the error metrics resemble closely the values obtained for the whole period. Again, the tendencies seen

previously can be seen in Table V, apart from the positive mean bias error for H_{m0}. The values of the error metrics show that the model is less performing for the spring season. For the summer period, the mean bias error is not only negative: it oscillates between $[-0.045, 0.027]$ m for H_{m0}. The error metric values are also showing that the forecast model is performing better for this period with respect to the whole period and the spring and winter periods. For the autumn season, the mean bias error for H_{m0} follows the trend seen for the whole period. The values of the error metrics show that the model is performing better for this season than all other seasons.

The variation of the $RRMSE$ on a seasonal basis is depicted in Fig. 9 for H_{m0}. The $RRMSE$ is shown as a function of the forecast horizon for the four seasons and for all the data points. According to [12] the forecast is considered good if $RRMSE < 20\%$, fair if $20\% < RRMSE < 30\%$, and poor if $RRMSE > 30\%$. According to those criteria, the gray area on the figure can be considered as the limit of accuracy for the forecast model. The summer and autumn seasons of the last two years have been relatively calm. With this in mind, it can also be seen from Fig. 9 that the forecast model can better predict milder wave climate, as H_{m0} can be fairly predicted as far as 4.5 days ahead for those two seasons.

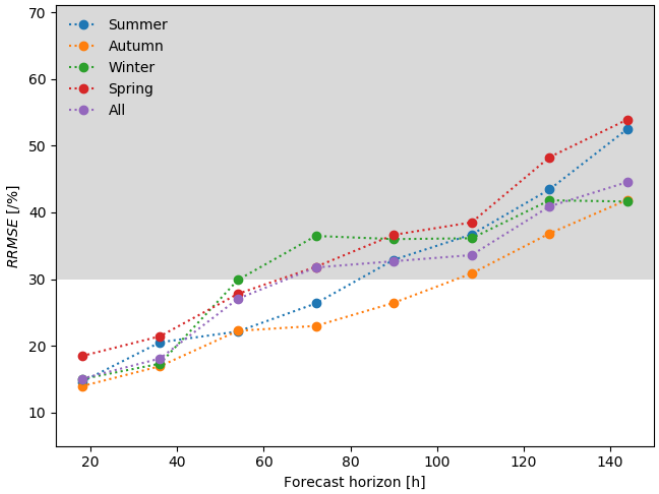

Fig. 9. $RRMSE$ of H_{m0} as a function of the forecast horizon for the four seasons. The $RRMSE$ as a function of the forecast horizon for the whole period is also shown. The grey area can be considered as the limit of accurate prediction for the forecast model.

IV. Conclusion

In this work, the forecast model for the DanWEC test center was introduced. The model is based on a hindcast model for the area, which has been validated using measured data from wave measuring buoys placed at the test center. The forecast model provides a 5½ days-horizon for a range of parameters enabling a better planning of O&M activities at the test center. An evaluation of the accuracy of the prediction given by the forecast model was performed. Several errors metrics were calculated and presented on a seasonal basis. Results have shown that the model is better at predicting wave heights than wave periods, and is mostly under predicting both H_{m0} and T_p. The model can be considered giving good prediction for a horizon of 2.5 days throughout the year and up to 5 days for some of the autumn and summer months.

Future work includes data assimilation from the wave measuring buoys into the forecast model in order to increase the accuracy of the prediction and thereby a better planning of the O&M at the test center.

Acknowledgement

The authors gratefully acknowledge the financial support from the Danish Energy Agency under The Energy Technology Development and Demonstration Program (EUDP) (Resource Assessment, Forecasts and WECs O&M strategies at DanWEC and beyond) which render this work possible.

References

[1] H. J. Brodersen, K. Nielsen, and J. P. Kofoed, "Development of the Danish test site DanWEC," In *10th European Wave and Tidal Energy Conference (EWTEC)*, Aalborg, Denmark, 2013.

[2] Danish Hydraulic Institute. "MIKE 21, Spectral Wave Module, Scientific Documentation," DHI. Hørsholm, Denmark, 2015. [Online] Available: http://manuals.mikepoweredbydhi.help/2017/Coast_and_Sea/M21SW_Scientific_Doc.pdf

[3] A. Tetu, and J. P. Kofoed. "Long-term wave climate at DanWEC," Department of Civil Engineering, Aalborg Univeristy. Aalborg, Denmark. DCE Contract Report No. 188, 2017.

[4] M. Rugbjerg, O. R. Sørensen, and V. Jacobsen, "Wave Forecasting For Offshore Wind Farms," In *9th International Workshop on Wave Hindcasting and Forecasting*, Victoria, B.C., Canada, 2006.

[5] K. Nielsen, M. Remmer, W. C. Beatie, "Elements of large wave power plants," In *1st European Wave and Tidal Energy Conference (EWTEC)*, Edinburgh, UK, 1993.

[6] Datawell BV. "Datawell Waves4 Manual, Software for Datawell Waverider buoys, User Manual," Datawell BV oceanographic instruments. Heerhugowaard, The Netherlands. 2018. [Online] Available: http://www.datawell.nl/Portals/0/Documents/Manuals/datawell_manual_waves4_user_2018-10-16.pdf

[7] MIKE 21 SW [Computer software]. DHI. Hørsholm, Denmark, 2019.

[8] R. E. Jensen, V. J. Cardone, and A. T. Cox, "Performance of third generation wave models in extreme hurricanes,". In *9th International Wind and Wave Workshop*, Victoria, B.C., Canada, 2006

[9] J. A. Battjes, and M. J. F. Stive, "Calibration and verification of a dispersion model for random breaking waves". *Journal of Geophysical Research*, vol. 112, pp. 307-319, 1985.

[10] G. Kaminsky, "Evaluation of depth-limited wave breaking criteria," In *2nd International Symposium on Ocean Wave Measurement and Analysis*, New Orleans, USA, 1993.

[11] P. M. Jensen, "DanWEC EUDP, Establishment of Wave Hindcast," DHI, Hørsholm, Denmark. Technical report, 2016.

[12] M.-F Li, X.-P. Tang, W. Wu and H.B. Liu, "General models for estimating daily global solar radiation for different solar radiation zones in mainland China," *Energy Conversion and Management*, vol. 70, pp. 139-148, 2013.